

A Sugar-Functionalized Amphiphilic Pillar[5]arene: Synthesis, Self-Assembly in Water, and Application in Bacterial Cell Agglutination

Guocan Yu,[†] Yingjie Ma,[†] Chengyou Han,[†] Yong Yao,[†] Guping Tang,[§] Zhengwei Mao,[‡] Changyou Gao,[‡] and Feihe Huang^{*,†}

[†]Department of Chemistry and [‡]Department of Polymer Science and Engineering, MOE Key Laboratory of Macromolecular Synthesis and Functionalization, Zhejiang University, Hangzhou 310027, P. R. China

[§]Department of Chemistry, Institute of Chemical Biology and Pharmaceutical Chemistry, Zhejiang University, Hangzhou 310027, P. R. China

S Supporting Information

ABSTRACT: A novel sugar-functionalized amphiphilic pillar[5]arene containing galactose groups as the hydrophilic part and alkyl chains as the hydrophobic part was designed and synthesized. It self-assembles in water to produce nanotubes as confirmed by TEM, SEM, and fluorescence microscopy. These nanotubes, showing low toxicity to both cancer and normal cells, can be utilized as excellent cell glues to agglutinate *E. coli*. The existence of galactoses on these nanotubes provides multivalent ligands that have high affinity for carbohydrate receptors on *E. coli*.

Considerable attention has been devoted to understanding and mimicking bacterial adhesion-specific interactions for various purposes, such as pathogen detection and the inhibition of bacterial infections via the chemotactic responses of bacteria toward the corresponding ligands.¹ Generally, pathogens bind to carbohydrates existing on the host cells they infect. Carbohydrate–protein interactions typically exhibit high specificity and weak affinities toward the corresponding ligands or receptors, always in the millimolar range.² In order to produce glycotherapeutics and diagnostic tools for antimicrobial therapy, targeted drug delivery and cell imaging, multivalency or cluster-glycoside effects are particularly well-documented to effectively enhance the affinity and selectivity in carbohydrate–protein interactions.³ In most cases, chemists have linked synthetic oligosaccharides to multivalent scaffolds (ranging from peptides, polymers, oligonucleotides, fullerenes, and calixarenes to dendrimers, nanoparticles, and arrays)⁴ through suitable “spacer” molecules to overcome the low binding affinities of monovalent glycosides.

However, contrary to the synthetic routines of oligonucleotides and peptides, the preparation of such complex glycomaterials can not be approached by any generalized protocols, and each target molecule represents an individual and challenging research project. Supramolecular self-assembly mediated by noncovalent forces,⁵ such as hydrogen bonding and hydrophobic, π – π stacking, electrostatic, and charge-transfer interactions, is an effective approach to construct desired architectures containing multivalent ligands, which can greatly reduce the need for tedious chemical syntheses. More importantly, the sizes, shapes, and functions of the self-assemblies can be easily controlled by changing the functional

or spacer groups, which play decisive roles in carbohydrate–protein interactions.⁶

Pillararenes, mainly including pillar[5]arenes⁷ and pillar[6]arenes,⁸ are linked by methylene (–CH₂–) bridges at *para*-positions of 2,5-dialkoxybenzene rings, forming a unique rigid pillar architecture, which is different from the basket-shaped structure of *meta*-bridged calixarenes. The unique symmetrical structure and easy functionalization of pillararenes have afforded them outstanding abilities to selectively bind different kinds of guests and provided a useful platform for the construction of various interesting supramolecular systems, including cyclic dimers,⁹ chemosensors,¹⁰ supramolecular polymers,¹¹ liquid crystals,¹² and transmembrane channels.¹³ However, the application of pillararenes in biologically relevant fields has not been reported.

Herein, we report the design and synthesis of a novel sugar-functionalized amphiphilic pillar[5]arene **P1** (Figure 1a) via the copper(I)-catalyzed alkyne–azide 1,3-dipolar cycloaddition (CuAAC) reaction (Scheme S2). Biocompatible galactoses were introduced as the hydrophilic part to endow the amphiphile excellent biological functions. Nanotubes were obtained by allowing an aqueous solution of **P1** to stand \sim 1 week, driven by van der Waals (vdW) interactions between the alkyl chains on the hydrophobic side and the intermolecular hydrogen bonds between the hydroxyls on the galactoses (Figure 1b). These nanotubes were utilized as excellent cell glues to agglutinate and inhibit the motility of pathogenic cells *E. coli*. The agglutination ability of the nanotubes was much higher than those of model compounds (**MC1** and **MC2**) and the parent water-soluble macrocyclic host **P2** (Figure 1a).

The critical aggregation concentration (CAC) of **P1** in water was calculated to be $\sim 2.48 \times 10^{-5}$ M by plotting the surface tension (γ) of the solution as a function of the concentration of **P1** (Figure S31). Similarly, the CAC value of the amphiphilic compound **MC1** was also obtained (1.01×10^{-5} M). However, the γ values of the solutions of **P2** and **MC2** remained almost unchanged at different concentrations, indicating that nanostructures did not form from them due to their excellent solubility in water (Figure S31).

Received: May 24, 2013

Published: June 24, 2013

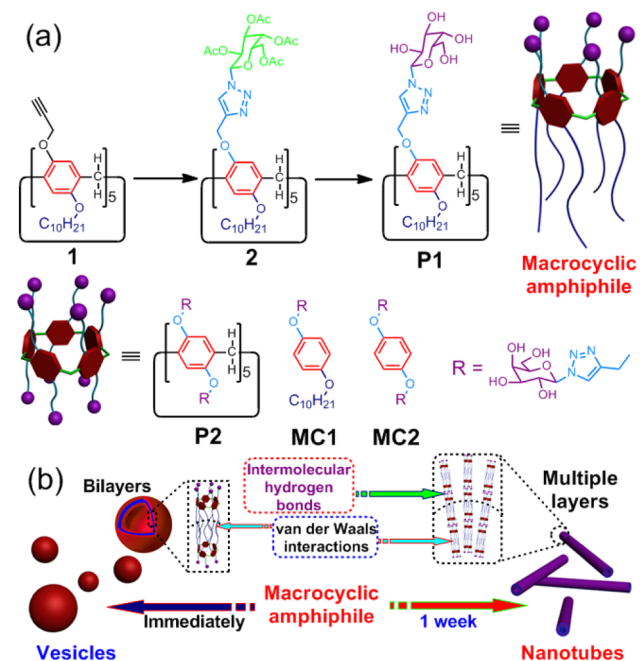


Figure 1. (a) Synthetic route to the macrocyclic amphiphile (**P1**) and chemical structures of the macrocyclic host (**P2**) and model compounds (**MC1** and **MC2**). (b) Schematic representation of the self-assembly process of **P1**.

For comparison, the self-assembly behavior of amphiphilic noncyclic monomeric analogue **MC1** in water was investigated first. Vesicles with the average diameter ~ 120 nm were observed in TEM image (Figure 2a), which was confirmed by a dynamic light scattering (DLS) experiment (Figure S35a). It should be noted that the vesicles formed by **MC1** were quite stable and did not transform into other structures even after 2 weeks (Figure

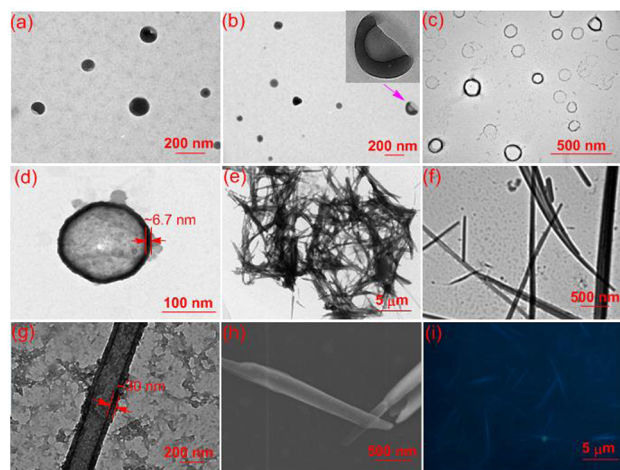


Figure 2. TEM images: Vesicles formed from **MC1** (a) 5 min after it was poured into water and (b) after standing the solution for 2 weeks (both scale bars = 200 nm) with an inset showing an enlarged vesicle pointed out by a purple arrow. (c) Vesicles formed from **P1** 5 min after it was poured into water (scale bar = 500 nm). (d) Enlarged image of a vesicle (scale bar = 100 nm). (e) Nanotubes formed from **P1** after standing the solution for 1 week (scale bar = 5 μ m). Enlarged images of (e) with scale bars = (f) 500 nm and (g) 200 nm. (h) SEM image of the nanotubes (scale bar = 500 nm). (i) Fluorescence microscopic image of the nanotubes with pyrene loaded ($\lambda_x = 360$ nm, scale bar = 5 μ m). Initial concentrations of **P1** and **MC1** were 50 μ M.

2b). Then, DLS, SEM, and TEM were employed to investigate the self-assembly of the macrocyclic amphiphile **P1**. As shown in Figure 2c, when **P1** was dissolved in water with a concentration of 5.0×10^{-5} M, which was higher than its CAC value, vesicles with the average diameter of ~ 150 nm were observed. The thickness of the vesicles was calculated to be ~ 6.7 nm (Figure 2d). Notably, the extended length of the **P1** is ~ 3.2 nm (Figure S32), close to half the thickness of the vesicles, indicating **P1** self-assembled into vesicles in a bilayer packing mode. Moreover, calcein could be wrapped up by the vesicles (Figure S34c), confirming that the vesicles were hollow. As shown by DLS investigation, the main diameter distribution of the vesicles was ~ 170 nm (Figure S35b), in agreement with the TEM images in Figure 2c,d. It should be pointed out that the diameter of the vesicles measured by DLS was a little larger than that obtained from the TEM images, attributable to swelling of the spherical structures in water.^{5i,k}

Notably, black floccules were clearly observed in an aqueous solution of **P1** after 1 week (Figure S36b) and became larger as the standing time increased. The aggregation behavior of **P1** in water as a function of time was investigated by UV-vis spectroscopy (Figure S36). The peak at ~ 285 nm ascribed to the characteristic absorbance of **P1** decreased due to the formation of floccules. On the contrary, almost no changes were observed in the UV-vis spectra corresponding to the absorption of **MC1** even after 2 weeks (Figure S37), indicating that the pillar[5]arene frame plays an important role in the self-assembly process of **P1**. The morphology of the floccules displayed by the TEM images was regular nanotubes 100–200 nm in diameter and several micrometers in length (Figure 2e–g). The coexistence of vesicles and short nanotubes could also be observed after standing the solution for 4 days (Figure S34d), demonstrating the gradual transformation from vesicles to nanotubes by increasing the standing time. The thickness of the nanotubes was ~ 30 nm (Figures 2g and S34f), indicating a multiple-layer structure of the nanotubes (Figure 1b). SEM was also utilized to confirm the tubular structure of the self-assemblies (Figure 2h), which was consistent with the TEM results. In order to further demonstrate the successful transformation from the vesicles to the nanotubes, pyrene was used as a probe to penetrate into the hydrophobic region in the wall of the nanotubes composed of alkyl chains through hydrophobic interactions. As shown in Figure 2i, tubular assemblies formed by **P1** could be clearly seen, which certified the existence of nanotubes.

Furthermore, FTIR spectroscopy (Figure S38) was utilized to provide convincing insights into the interactions between the macrocyclic amphiphile, which were extremely important for the self-assembly process. Compared with the spectrum corresponding to the powder form of **P1**, the absorption of the nanotubes related to the O–H stretching vibration shifted to lower wavenumber (from 3390 to 3369 cm^{-1} , Figure S38), in agreement with the participation of hydrogen bonding in the aggregation process,¹⁴ a key factor in the formation of nanotubes. On the other hand, the FTIR spectra in Figure S33 showed that the C–H stretching and rocking bands shifted from 2926, 2855, and 1234 cm^{-1} to 2920, 2851, and 1209 cm^{-1} , respectively, after the formation of nanotubes. This result provided reliable evidence to confirm effective achievement of vdW interactions between the alkyl chains in the nanotubes,¹⁴ which is another crucial driving force for the transformation of the vesicles to the nanotubes and the stabilization of the supramolecular structures.

It is a spontaneous dynamic process for an amphiphilic molecule to aggregate in water when the concentration reaches or exceeds its CAC value.^{5g} Moreover, the microassembled structures of the aggregates formed by the building blocks are determined by the curvature of the membrane.^{5i,k} Typically, low membrane curvature favors forming a vesicular structure, while high membrane curvature tends to form a nanotubular structure. In our system, the membrane curvature was enhanced by introducing a rigid segment into the macrocyclic amphiphile **P1**, resulting in the formation of nanotubes.^{7d} This phenomenon was quite different from the self-assembly behavior of **MC1** which tended to form vesicles, proving that the pentagon-like cyclic pillar[5]arene structure played a crucial role in the fabrication of multidimensional self-assemblies and the stability of the aggregates formed by **P1**.

In order to apply a compound in biologically relevant fields, its toxicity should be evaluated. From hematoxylin and eosin (H&E) staining experiments and 3-(4',5'-dimethylthiazol-2-yl)-2,5-diphenyl tetrazolium bromide (MTT) assays (see Figure S39), **MC1**, **MC2**, **P1**, and **P2** showed low toxicity to both cancer cells (A549, a kind of lung cancer cells) and normal cells (Chinese hamster lung fibroblast cell), demonstrating that these compounds could be utilized in biorelated fields.

As mentioned above, cell-surface carbohydrates are exploited by many pathogens for adherence to tissues and entry into host cells. The interactions taking place at cell–cell interfaces occur simultaneously due to multiple binding events which can effectively amplify affinities relative to interactions that involve only a single ligand. This effect has led to the development of multivalent antiadhesive therapeutics against bacteria and viruses. Recent reports have demonstrated that pathogenic cells can be agglutinated and that their motilities are inhibited effectively by multivalent carbohydrate-coated nanofibers.¹⁵

In our systems, the multivalent carbohydrate-coated nanotubes can be used as cell glues to study cell–cell interactions because they can accommodate multivalent bindings. As shown in Figure 3, no clusters of fluorescent bacteria were observed when *E. coli* was cultured with **MC2** (Figure 3b) and **P2** (Figure 3e). The reason was that their solubility was so good that multivalent ligands which are extremely important for the agglutination of bacterial cells could not form in water. TEM (Figure 3c,f) and optical microscopic images (Figure 3a,d) were also utilized to confirm whether *E. coli* agglutination was induced by **MC2** or **P2**. We found that only few *E. coli* cells contacted with each other when they were incubated with **MC2** or **P2**, indicating extremely low agglutination ability of these water-soluble compounds in the monovalent binding mode. Meanwhile, clusters of fluorescent bacteria with small sizes could be observed when *E. coli* were incubated with **MC1** (Figure 3h). TEM investigations provided convincing evidence for the agglutination of bacterial cells. As shown in Figure 3i, several *E. coli* cells contacted each other, because the galactoses on the outside of the vesicles provide binding sites for the receptors on *E. coli*. Furthermore, vesicles (pointed out by green arrows in Figure 3i) could be observed on the surfaces, strongly confirming our hypothesis. Interestingly, clusters of fluorescent bacteria with relatively large sizes were observed when *E. coli* was incubated with the **P1**-based nanotubes (Figure 3k), indicating strong interactions between the nanotubes and the pathogenic *E. coli* cells. Therefore, these **P1**-based nanotubes (pointed out by purple arrows in Figure 3l) could act as excellent cell glues to agglutinate *E. coli*, resulting in the formation of fluorescent bacteria clusters.

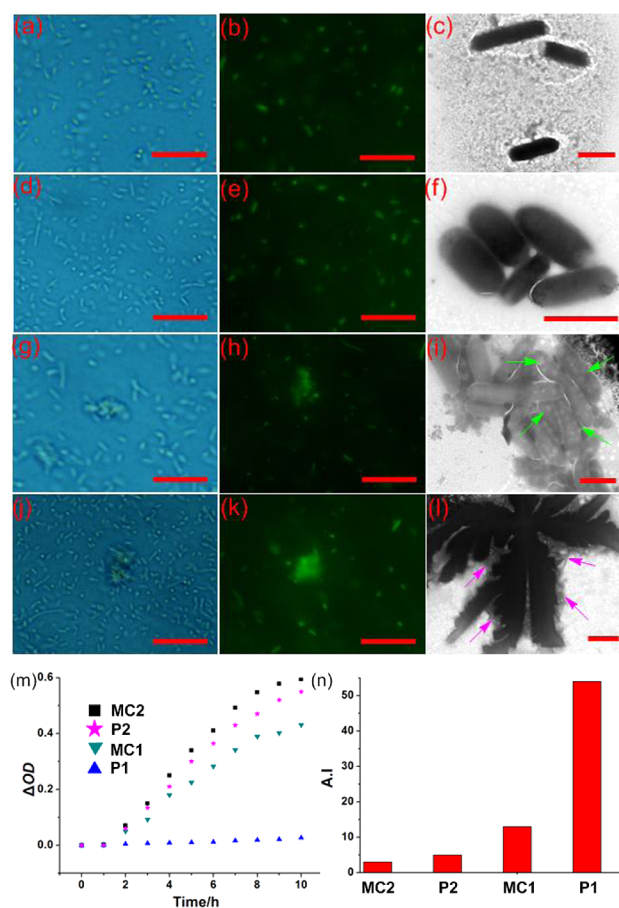


Figure 3. Microscopic images of *E. coli* agglutination incubated with **P1**, **P2**, **MC1**, and **MC2**, respectively (50.0 μM): (a) optical microscopic image (OMI) of **MC2**; (b) fluorescence microscopic image (FMI) of **MC2**; (c) TEM image (TEMI) of **MC2**; (d) OMI of **P2**; (e) FMI of **P2**; (f) TEMI of **P2**; (g) OMI of **MC1**; (h) FMI of **MC1**; (i) TEMI of **MC1**; (j) OMI of **P1**; (k) FMI of **P1**; (l) TEMI of **P1**. For OMI images, scale bar = 40 μm ; for FMI images, $\lambda_x = 360 \text{ nm}$, scale bar = 40 μm ; for TEMI images, scale bar = 2 μm . (m) Growth curves based on the optical density at 600 nm for *E. coli* grown in the presence of **P1**, **P2**, **MC1**, and **MC2**. (n) Agglutination index obtained from fluorescence microscopy and TEM images.

In order to further investigate the agglutination ability of the nanotubes, spectrophotometric analysis based on optical density was used to estimate the number of bacteria in liquid culture. As shown in Figure 3p, normal bacterial growth curves were observed for **MC2** and **P2**, indicating extremely low agglutination ability. Compared with **MC2** and **P2**, the agglutination ability of **MC1** was slightly stronger due to the formation of vesicles decorated by galactoses. More interestingly, we did not observe an increase in the cell population cultured with the **P1**-based nanotubes during our experimental time range, indicating that the bacteria were completely inhibited by the nanotubes. The length of the self-assemblies played a key role in the formation of bacterial clusters and was a crucial factor in controlling agglutination. For the nanotubes, the lengths can reach several micrometers, much longer than the average size of the vesicles formed by **MC1**, so they can interconnect more bacteria, resulting in the enhancement of the agglutination ability.

Moreover, we defined the average number of *E. coli* cells contacted with each other from 10 random fields of microscopic

images as the agglutination index (AI) to examine the abilities of the model compounds (MC1 and MC2) and the macrocyclic hosts (P1 and P2) to agglutinate bacterial cells (Figure 3n). A significant difference between the macrocyclic amphiphile P1 and the other three compounds was observed. The AI value of P1 was calculated to be 54, much higher than those of MC1 (13), MC2 (3), and P2 (5), in good agreement with the results obtained from the above-mentioned fluorescence microscopy, TEM, and spectrophotometric analyses. Clearly, these P1-based nanotubes exhibited excellent agglutination ability for *E. coli*.

In summary, we designed a novel sugar-functionalized amphiphilic pillar[5]arene P1 with galactoses as the hydrophilic part and alkyl chains as the hydrophobic part. Due to the existence of intermolecular hydrogen bonds between the galactoses and the vdW interactions between the alkyl chains, P1 self-assembled into vesicles in water and gradually transformed into nanotubes after standing for 1 week. The biocompatible galactoses coating the nanotubes endowed them with interesting biofunctions, which could act as excellent cell glues to effectively agglutinate *E. coli*. Compared with those of MC2 and P2 which have good solubility in water, the agglutination ability of the P1-based nanotubes was much higher due to the existence of multivalent ligands on their surfaces. For the amphiphilic model compound MC1 self-assembling into vesicles, its ability to agglutinate *E. coli* decreased dramatically due to the dimensional reduction of the aggregates. These results showed that supramolecular self-assemblies composed of rather simple ligands driven by noncovalent interactions are distinctive chemical tools for capturing living bacteria in solution. The structures, stability, and functions of the supramolecular self-assemblies can be easily controlled by introducing different functional groups through click chemistry, which have the potential to address many biocompatibility-related issues, opening up an even wider range of bioapplication opportunities in areas, such as drug delivery, bioconjugation, and specific recognition.

ASSOCIATED CONTENT

Supporting Information

Experimental details and characterization data. These material are available free of charge via the Internet at <http://pubs.acs.org>.

AUTHOR INFORMATION

Corresponding Author

fhuang@zju.edu.cn

Notes

The authors declare no competing financial interest.

ACKNOWLEDGMENTS

This work was supported by National Basic Research Program (2013CB834502), the National Natural Science Foundation of China (91027006 and 21125417), and the Fundamental Research Funds for the Central Universities (2012QNA3013).

REFERENCES

(1) (a) Lindhorst, T. K. *Top. Curr. Chem.* **2002**, *218*, 201. (b) Gu, L.; Elkin, T.; Jiang, X.; Li, H.; Lin, Y.; Qu, L.; Tzeng, T.-R. J.; Joseph, R.; Sun, Y.-P. *Chem. Commun.* **2005**, 874. (2) (a) Rudd, P. M.; Elliott, T.; Cresswell, P.; Wilson, I. A.; Dwek, R. A. *Science* **2001**, *291*, 2370. (b) Gestwicki, J. E.; Cairo, C. W.; Strong, L. E.; Oetjen, K. A.; Kiessling, L. L. *J. Am. Chem. Soc.* **2002**, *124*, 14922. (c) Disney, M. D.; Zheng, J.; Swager, T. M.; Seeberger, P. H. *J. Am. Chem. Soc.* **2004**, *126*, 13343. (d) Crocker, P. R.; Paulson, J. C.; Varki, A.

Nat. Rev. Immunol. **2007**, *7*, 255. (e) Park, S.; Lee, M.-R.; Shin, I. *Chem. Soc. Rev.* **2008**, *37*, 1579.

(3) (a) Rüdiger, H.; Gabius, H.-J. *Glycoconjugate J.* **2001**, *18*, 589. (b) Fuster, M. M.; Esko, J. D. *Nat. Rev. Cancer* **2005**, *5*, 526. (c) van Kooyk, Y.; Rabinovich, G. A. *Nat. Immunol.* **2008**, *9*, 593.

(4) (a) Lee, Y. C.; Lee, R. T. *Acc. Chem. Res.* **1995**, *28*, 321. (b) Baldini, L.; Casnati, A.; Sansone, F.; Ungaro, R. *Chem. Soc. Rev.* **2007**, *36*, 254. (c) Dondoni, A.; Marra, A. *Chem. Rev.* **2010**, *110*, 4949. (d) Kiviniemi, A.; Virta, P.; Drenichev, M. S.; Mikhailov, S. N.; Lonnberg, H. *Bioconjugate Chem.* **2011**, *22*, 1249. (e) Durka, M.; Buffet, K.; Iehl, J.; Holler, M.; Nierengarten, J. F.; Vincent, S. P. *Chem.—Eur. J.* **2012**, *18*, 641.

(5) (a) Zimmerman, S. C.; Wendland, M. S.; Rakow, N. A.; Zharov, I.; Suslick, K. S. *Nature* **2002**, *418*, 399. (b) Huang, F.; Fronczek, F. R.; Gibson, H. W. *J. Am. Chem. Soc.* **2003**, *125*, 9272. (c) Huang, F.; Gibson, H. W. *J. Am. Chem. Soc.* **2004**, *126*, 14738. (d) Kim, K.; Selvapalam, N.; Ko, Y. H.; Park, K. M.; Kim, D.; Kim, J. *Chem. Soc. Rev.* **2007**, *36*, 267. (e) Schmuck, C.; Rehm, T.; Klein, K.; Gröhn, F. *Angew. Chem., Int. Ed.* **2007**, *46*, 1693. (f) Jiang, W.; Schäfer, A.; Mohr, P. C.; Schalley, C. A. *J. Am. Chem. Soc.* **2010**, *132*, 2309. (g) Helttunen, K.; Shahgaldian, P. *New J. Chem.* **2010**, *34*, 2704. (h) Chen, Y.; Guan, Z. *J. Am. Chem. Soc.* **2010**, *132*, 4577. (i) Yu, G.; Xue, M.; Zhang, Z.; Li, J.; Han, C.; Huang, F. *J. Am. Chem. Soc.* **2012**, *134*, 13248. (j) Wang, C.; Wang, Z.; Zhang, X. *Acc. Chem. Res.* **2012**, *45*, 608. (k) Yu, G.; Zhou, X.; Zhang, Z.; Han, C.; Mao, Z.; Gao, C.; Huang, F. *J. Am. Chem. Soc.* **2012**, *134*, 19489. (l) Zhu, K.; Vukotic, V. N.; Loeb, S. J. *Angew. Chem., Int. Ed.* **2012**, *51*, 2168. (m) Vinciguerra, B.; Cao, L.; Cannon, J. R.; Zavalij, P. Y.; Fenselau, C.; Isaacs, L. *J. Am. Chem. Soc.* **2012**, *134*, 13133.

(6) (a) Dimick, S. M.; Powell, S. C.; McMahon, S. A.; Moothoo, D. N.; Naismith, J. H.; Toone, E. J. *J. Am. Chem. Soc.* **1999**, *121*, 10286. (b) Müller, M. K.; Brunsveld, L. *Angew. Chem., Int. Ed.* **2009**, *48*, 2921. (c) Deniaud, D.; Julienne, K.; Gouin, S. G. *Org. Biomol. Chem.* **2011**, *9*, 966. (d) Lee, D.-W.; Kim, T.; Park, I.-S.; Huang, Z.; Lee, M. *J. Am. Chem. Soc.* **2012**, *134*, 14722.

(7) (a) Ogoshi, T.; Kanai, S.; Fujinami, S.; Yamagishi, T. A.; Nakamoto, Y. *J. Am. Chem. Soc.* **2008**, *130*, 5022. (b) Zhang, Z.; Xia, B.; Han, C.; Yu, Y.; Huang, F. *Org. Lett.* **2010**, *12*, 2385. (c) Li, C.; Zhao, L.; Li, J.; Ding, X.; Chen, S.; Zhang, Q.; Yu, Y.; Jia, X. *Chem. Commun.* **2010**, 46, 9016. (d) Yao, Y.; Xue, M.; Chen, J.; Zhang, M.; Huang, F. *J. Am. Chem. Soc.* **2012**, *134*, 15712. (e) Chen, Y.; Cao, D.; Wang, L.; He, M.; Zhou, L.; Schollmeyer, D.; Meier, H. *Chem.—Eur. J.* **2013**, *19*, 7064.

(8) (a) Cao, D.; Kou, Y.; Liang, J.; Chen, Z.; Wang, L.; Meier, H. *Angew. Chem., Int. Ed.* **2009**, *48*, 9721. (b) Cragg, P. J.; Sharma, K. *Chem. Soc. Rev.* **2012**, *41*, 597. (c) Xue, M.; Yang, Y.; Chi, X.; Zhang, Z.; Huang, F. *Acc. Chem. Res.* **2012**, *45*, 1294. (d) Yu, G.; Han, C.; Zhang, Z.; Chen, J.; Yan, X.; Zheng, B.; Liu, S.; Huang, F. *J. Am. Chem. Soc.* **2012**, *134*, 8711.

(9) (a) Zhang, Z.; Yu, G.; Han, C.; Liu, J.; Ding, X.; Yu, Y.; Huang, F. *Org. Lett.* **2011**, *13*, 4818. (b) Liu, L.; Wang, L.; Liu, C.; Fu, Z.; Meier, H.; Cao, D. *J. Org. Chem.* **2012**, *77*, 9413.

(10) (a) Yu, G.; Zhang, Z.; Han, C.; Xue, M.; Zhou, Q.; Huang, F. *Chem. Commun.* **2012**, 48, 2958. (b) Strutt, N. L.; Forgan, R. S.; Spruell, J. M.; Botros, Y. Y.; Stoddart, J. F. *J. Am. Chem. Soc.* **2011**, *133*, 5668.

(11) (a) Zhang, Z.; Luo, Y.; Chen, J.; Dong, S.; Yu, Y.; Ma, Z.; Huang, F. *Angew. Chem., Int. Ed.* **2011**, *50*, 1397. (b) Guan, Y.; Ni, M.; Hu, X.; Xiao, T.; Xiong, S.; Lin, C.; Wang, L. *Chem. Commun.* **2012**, 48, 8532. (c) Xia, B.; Zheng, B.; Han, C.; Dong, S.; Zhang, M.; Hu, B.; Yu, Y.; Huang, F. *Polym. Chem.* **2013**, *4*, 2019.

(12) Nierengarten, I.; Guerra, S.; Holler, M.; Nierengarten, J.-F.; Deschenaux, R. *Chem. Commun.* **2012**, 48, 8072.

(13) Si, W.; Chen, L.; Hu, X.-B.; Tang, G.; Chen, Z.; Hou, J.-L.; Li, Z.-T. *Angew. Chem., Int. Ed.* **2011**, *50*, 12564.

(14) Nebot, V. J.; Armengol, J.; Smets, J.; Prieto, S. F.; Escuder, B.; Miravet, J. F. *Chem.—Eur. J.* **2012**, *18*, 4063.

(15) (a) Ryu, J.-H.; Lee, E.; Lim, Y.; Lee, M. *J. Am. Chem. Soc.* **2007**, *129*, 4808.